UNSYS digital

The Journal of Instrumentation, Automation and Systems

Development of L-band Circularly Polarized Synthetic Aperture Radar System

Yuta Izumi†, Zafri Bin Baharuddin†, Heein Yang†, Hendra Agus† and Josaphat Tetuko Sri Sumantyo†

†Center for Environmental Remote Sensing, Chiba University, Japan

Abstract—In recent years, Synthetic aperture radar (SAR) has obtained various information on the Earth surface by use of polarimetric SAR which can obtain polarimetric information. Conventional SAR employs linearly polarized (LP) RF signals but a drawback of LP signals is that it is easily affected by the Faraday rotation effect. This distorts the signal amplitude as the signal traverses the ionosphere which results in antenna misalignment. This paper presents the development of a SAR system that adopts circular polarization (CP) to compensate the alignment problem in LP-SAR. To evaluate performance of the developed CP-SAR system, we measured transmit signals and conducted imaging test. For the imaging test, canonical targets were imaged in an anechoic chamber using inverse SAR (ISAR) measurement geometry. The results indicate that the proposed CP-SAR system can measure and form SAR images using circular polarization.

Keywords—Synthetic aperture radar, circular polarization, Faraday rotation, inverse synthetic aperture radar.

doi: 10.21535/jias.v3i1.902

I. Introduction

SYNTHETIC aperture radar (SAR) is an active radar that is transmitted and detected sequentially along a flight path. The total received signals on the flight path are combined in process called range and azimuth compression to generate target image. SAR data has been applied for observation and study of the Earth surface, for example, in natural disasters, land subsidence, and so on. SAR is usually mounted on a platform such as a satellite or an aircraft. Conventional satellite onboard SAR systems employ linearly polarized (LP) antenna. One problem of space-borne SAR is that LP signals are affected by the Faraday rotation effect, where reference plane of transmitted microwave rotates as it propagates through the Earth's ionosphere. This phenomenon frequently occurs in case of the LP microwave, particularly at lower frequencies [1]. Until now, many satellites onboard SAR have utilized LP antenna at low frequencies. For example, the Advanced Land Observing Satellite (ALOS) phased array type L-band SAR (PALSAR) operates in the L-band frequency (1.27 GHz) while the Environmental Satellite (ENVISAT) Advanced SAR (ASAR) operates in C-band (5.331 GHz) [2], [3]. Therefore, distortion compensation methods for the received LP data are necessary in post processing stage such as one proposed by Freeman [1]. On the other hand, it has been shown that the Faraday rotation has negligibly effect on circularly polarized (CP) microwave signal [4]. Additionally, for oceanic ship detection, CP performs better detection at lower incidence angles, as discussed by R. Touzi [5].

Thus, this paper proposes a fully polarimetric circularly polarized (CP) SAR system for L-band that employs CP antennas [6], [7]. We present an experimental validation of the proposed L-band CP-SAR system. Section II explains the CP-SAR system structure and a qualitative performance analysis of the generated chirp signal to be transmitted. Section III presents setup for SAR imaging in an anechoic chamber and evaluates performance of the proposed CP-SAR system and its SAR image results.

II. Structure of The Proposed CP-SAR

The proposed CP-SAR system consists of PC, chirp signal generator implemented on a field programmable gate array (FPGA), analog-to-digital converter/digital-to-analog converter (ADC/DAC), L-band (1.27GHz) radio frequency (RF) transmitter/receiver, and micro-strip CP antennas. In the proposed system, the PC manages the system behavior and also processes SAR raw data using MATLAB.

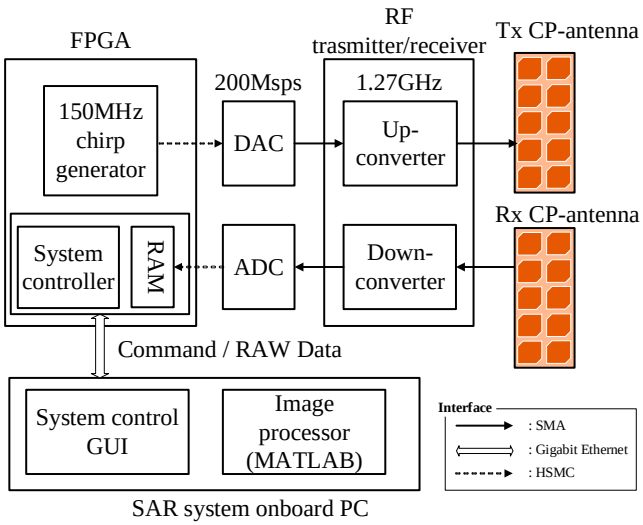

Figure 1 L-band CP-SAR system block diagram

Corresponding author: Yuta Izumi (e-mail: yutalimit@gmail.com).
This paper was submitted on March 14, 2016; revised on May 22, 2016; and accepted on June 05, 2016.

The chirp signal is generated by the chirp signal generator and then up-converted by the RF transmitter before being transmitted by the antenna. Chirp signal is a linearly frequency modulated (LFM) wave with its instantaneous frequency increasing or decreasing linearly with time [8]. It is widely used as transmission signal in pulse compressed radar. Chirp signal design is important as different chirp signals can provide different scattering information. Block diagram of the proposed SAR system and specification are shown in **Figure 1** and **Table 1** respectively.

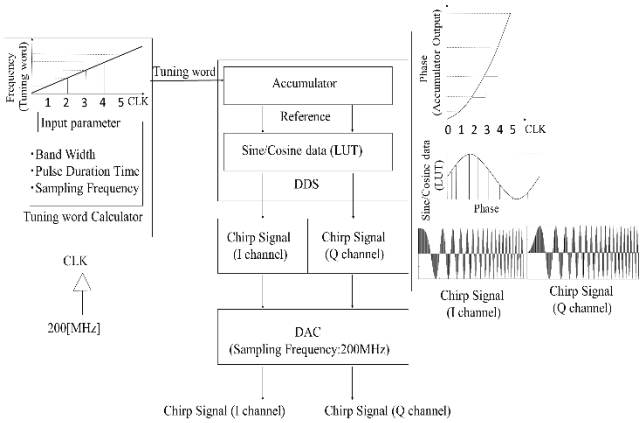

Figure 2 Structure of developed direct digital synthesizer (DDS)

A. Chirp signal generator

The chirp generator creates signal that is defined using following equation

$$S(t) = \mathrm{rect}\left(\frac{t}{\mathrm{T}}\right)\exp(\mathrm{j}\pi K t^2), \tag{1}$$

where T is pulse duration time, and K is chirp rate which is expressed by

$$K = \frac{B}{\mathrm{T}}, \tag{2}$$

where B is frequency bandwidth [9], [10]. Phase (ϕ) and instantaneous frequency (f) of the chirp signal are shown as

$$\phi(t) = \pi K t^2, \tag{3}$$

$$f(t) = \frac{1}{2\pi}\frac{d\phi}{dt} = Kt. \tag{4}$$

As defined in (1), the chirp signal can be expressed as a complex number where real part of the chirp signal is in-phase (I), and imaginary part is quadrature (Q). From (3) and (4), the chirp phase and the instantaneous frequency are expressed as second-order and first-order functions of time.

For digital chirp signal generator, memory-map based and direct digital synthesizer (DDS) chirp signal generators are widely used. The memory-map based chirp signal generator reads the discrete chirp signal which is stored in a read only memory (ROM). Hence if several types of wide bandwidth chirp signal are required, large memory capacity would be necessary. The DDS chirp signal generator generates phase component of chirp signal using input parameters and reads corresponding amplitude value which is stored in sine/cosine look-up table (LUT) [8], [11]. Therefore, the DDS can generate the desired chirp signal in real-time using two LUTs, and also it can save the ROM size. The DDS which is implemented on the FPGA is able to flexibly change the chirp signal bandwidth.

The first DDS chirp signal generator was proposed by P. C. Pedersen [8]. The Pedersen's DDS is widely used as basic method of DDS. The developed DDS consists of phase accumulator and ROM, as shown in Fig.2. The implemented phase accumulator works as a discrete counter to generate phase value. The ROM inside of the chirp generator stores discrete sine/cosine wave as a LUT. In the beginning of process, the DDS calculates tuning word which can be considered as frequency component of the chirp signal because it is expressed as first-order function of time. Tuning word (M) is calculated as

$$M(t) = \mathrm{rect}\left(\frac{t}{\mathrm{T}}\right)\frac{B}{f_{\mathrm{clk}}}2^n \quad t\left[-\frac{\mathrm{T}}{2},\frac{\mathrm{T}}{2}\right], \tag{5}$$

where f_{clk} is clock frequency of the DDS circuit and n is bit number [9]. After the DDS calculates the tuning word, it accumulates the calculated tuning word to generate the phase components of the chirp signal. Finally, the corresponding amplitudes are read from LUTs according to the calculated phase values. Output chirp signal frequency (f_{out}) is expressed as

$$f_{\mathrm{out}} = \frac{f_{\mathrm{clk}}}{2^n}. \tag{6}$$

This paper assumes that the clock frequency (f_{clk}) is set to 200MHz.

B. RF transmitter/receiver

Because a chirp is expressed by complex number, RF transmitter/receiver needs two input parameters, which are the real and imaginary parts, to construct one chirp signal. Thus IQ modulation method is used in order for I and Q to coexist in the microwave. When receiving signals, the radio waves can also be separated into the respective I and Q channels. As such, the I and Q signal forms composites for pulse compression. A structure of our RF transmitter/receiver is shown in **Figure 3**.

TABLE I CP-SAR SYSTEM SPECIFICATION

Category	Specification
Center frequency	1270 MHz
Maximum bandwidth	150 MHz
Polarization	LHCP/RHCP
Peak output power	50 W

A. Circularly polarized antenna

Compared to conventional LP-SAR, the biggest difference in our system is antenna polarization. CP antennas were utilized with the system in this paper. Since our SAR system is to be mounted on a satellite or unmanned aerial vehicle (UAV), lightweight antennas are preferred [12]. Due to this reason, the antenna was fabricated using micro-strip substrates [13]. These antennas satisfy the CP performance requirement with a corner truncated patch array, as shown in **Figure 4**. In order to operate with full polarimetry, left-handed circularly polarized (LHCP) antennas and right-handed circularly polarized (RHCP) antennas were both fabricated. The CP antenna specification is shown in **TABLE II**.

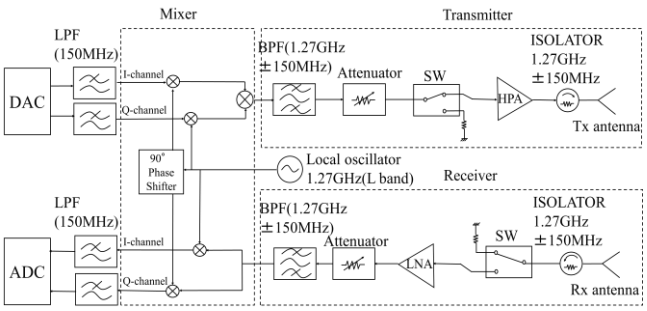

Figure 3 The RF transmitter/receiver structure. Local oscillator generates a 1.27 GHz (L-band) frequency

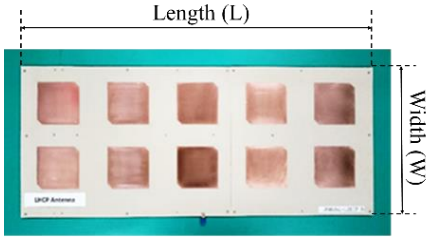

Figure 4 Radiating layer of LHCP fabricated micro-strip patch array antenna with corner truncated for CP radiation

TABLE II CIRCULARLY POLARIZED ANTENNA SPECIFICATION

Parameter	Specification
Impedance bandwidth, S11	58 MHz
Axial ratio (AR)	3 dB< for ±20°from main-beam 3dB< for 1.252-1.27GHz
Antenna gain	13.4 dBic
Antenna aperture (LxW)	655.0 x 285.0 mm
3-dB Azimuth beam-width	20.0°

B. Behavior of the proposed CP-SAR system

To manage the whole system, the system controller which works as state machine was implemented on the FPGA. Once it gets a command from the PC, the system starts to work inside of the state machine shown in **Figure 5**. Transmission and reception of the pulse are performed in the RUN-state. To check the signal or to perform a measurement, the proposed CP-SAR system has three operation modes: test-mode, measurement-mode, and observation-mode. During the test-mode, the system transmits and receives a single chirp signal to conduct a point target test. The measurement-mode sends continuous pulses according to pulse repetition interval (PRI) to measure output pulses by using external instrument such as an oscilloscope or a spectrum analyzer. The last mode is the observation mode, where the system automatically transmits and receives the signal with prescribed number of times according to PRI.

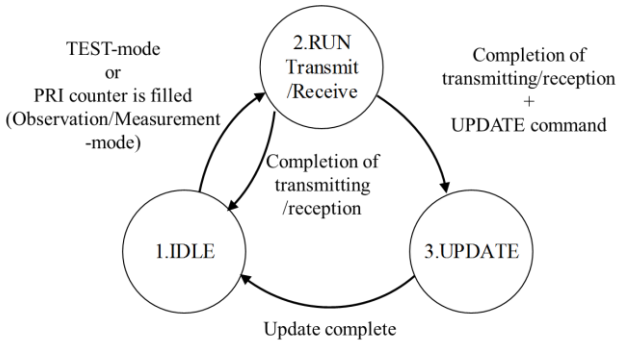

Figure 5 CP-SAR system state machine: IDLE, RUN and UPDATE states implemented in the FPGA

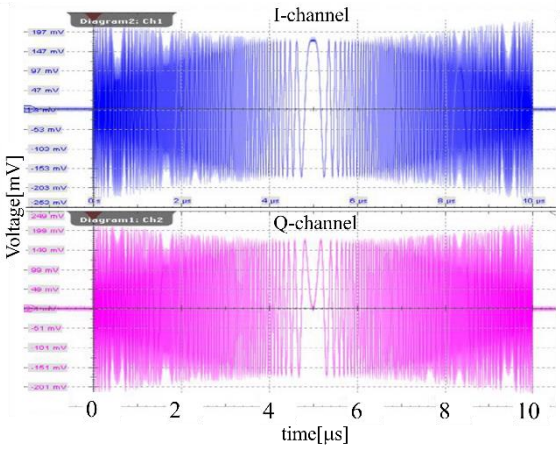

Figure 6 Measured I and Q chirp signals in time domain. Both signals were observed at the DAC output by setting bandwidth to 150 MHz, and pulse duration time to 10 μs

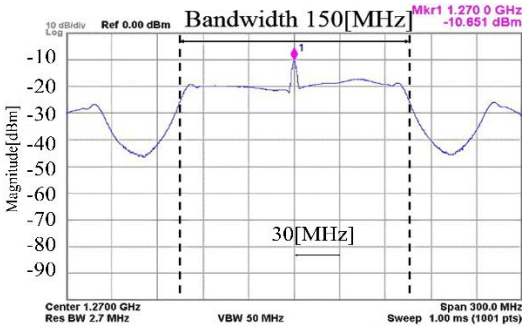

Figure 7 A chirp signal in frequency domain from the RF transmitter output, with settings of bandwidth 150 MHz, pulse duration time 2μs, and via 40 dB attenuator

C. The signal measurement environment

Chirp signal at baseband and L-band frequency were measured using both an oscilloscope and a spectrum analyzer to validate the quality of output signals. According to the requirement of our SAR system, the chirp signal set to 150 MHz bandwidth and 10μs pulse duration time were measured. Fig.6 shows the measured DAC output of the chirp signal in time domain. From this figure, noises are not visible and pulse duration time is observed exactly 10 μs. **Figure 7** shows result of RF transmitter output in frequency domain. This result indicates that the up-converted chirp pulse achieves the required 150 MHz bandwidth in approximately -30 dBm.

III. SAR MEASUREMENT IN ANECHOIC CHAMBER

This section presents SAR measurement in an anechoic chamber to verify the CP-SAR system performance. Purpose of this experiment is to generate SAR images based on the point target analysis using canonical reflectors. Our SAR measurement setup is shown in **Figure 8** and **Figure 9**. In this experiment, inverse SAR (ISAR) test was conducted where target moves along azimuth direction instead of the radar system. To generate the images, this experiment adopts stop-and-go model where the SAR system operates only during stop position at every azimuth points. The generated images were analyzed by range resolution (δ_r) and azimuth resolution (δ_a) which are given by the following equations [14]

$$\delta_r = \frac{c}{2B}\cos\phi\,, \tag{7}$$

$$\delta_a = \frac{c}{2L_{syn}f}\sqrt{\left(\frac{L_{syn}}{2}\right)^2 + R_0{}^2}\,, \tag{8}$$

where c is the speed of light, ϕ is antenna elevation angle, L_{syn} is synthetic aperture length, f is center of frequency, and R_0 is range distance.

A. Experiment geometry and parameters

The target on the platform moves 2.25m along on rail with azimuth interval of 0.05 m. The antenna was set up as quasi-monostatic configuration due to large size of the L-band micro-strip patch array antennas. The antennas and reflectors were placed at the same height, and distance between them was approximately 4 meters. The experiment concept is based on full-polarimetry to get co-polarization (LR, RL) and cross-polarization (LL, RR) channels data. For convenience, this paper defines scattering order as transmission and reception. For example, RL channel indicates RHCP transmission and LHCP reception. For the targets, an aluminum plate and vertical dihedral corner reflectors were chosen for measuring surface scattering and double scattering echoes, as shown in Fig.10. In general, the corner reflector's aperture size is required to be larger than 10λ for far field outdoor experiments, where λ is wavelength [15]. Since the experiment was conducted in an indoor anechoic chamber, the chosen reflector size was smaller than 10λ. Table.3 notes several system parameters that were used in the experiment.

We first measured empty room without any target to calibrate the system. This was then followed by SAR measurements using all polarization channels, one target at a time. The PC saves measured I and Q scattering signals for processing and image reconstruction.

B. Result and Discussion

Figure 11 shows CP-SAR images generated from the experiment. These images were processed by range-Doppler algorithm (RDA) using the MATLAB [16]. For matched filtering process in range domain, theoretical transmitted signal was applied as reference signal for pulse compression. The receiving signal was successfully compressed in the RDA algorithm. In the same manner, azimuth compression was also done. These images in **Figure 11** are normalized to maximum signal strength in one set of polarization. Some noises were detected due to multiple scattering between the reflector and antennas because both are made of metal, as shown in the bounding box of **Figure 11** (a).

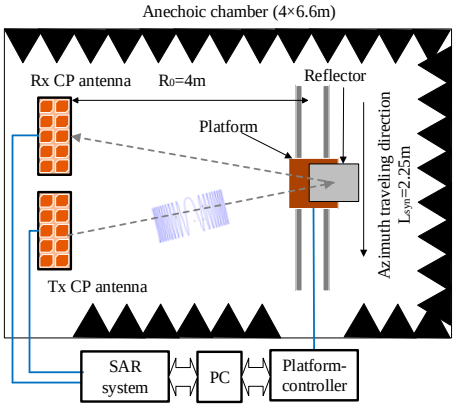

Figure 8 Experiment concept inside of the 4 x 6.6 m anechoic chamber. The experiment setup consists of the SAR system, the PC, the platform-controller, the CP-antenna, the platform, and the reflector.

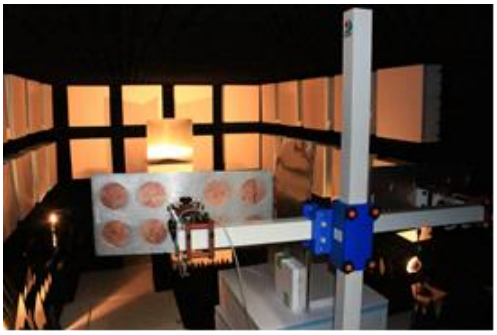

Figure 9 A plate type aluminum reflector target and CP antenna set-up inside the anechoic chamber.

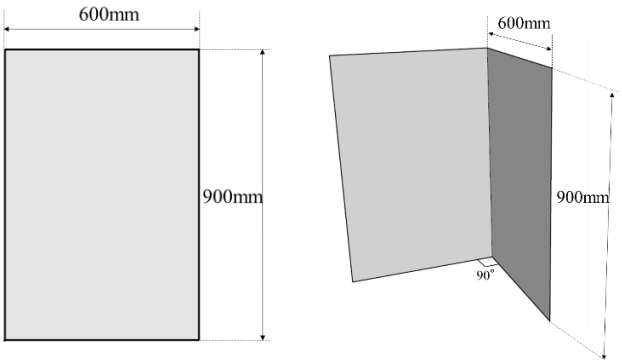

Figure 10 The aluminum reflectors: (a) Plate type (b) Vertical dihedral type with 90° angle of both faces.

Theoretically, peak power of each images are different according to polarization channels [17]. However, the experimental images were not able to confirm the peak value difference between each images because our micro-strip patch array antenna has small bandwidth 18MHz. Based on that reason, part of the chirp signal became elliptical polarized wave. To improve our work, we need to fabricate micro-strip antenna with perfect AR (0dB) in wide frequency range.

One evaluation criteria of the experiment and the proposed system is image resolution. **TABLE IV** shows range resolution and azimuth resolution which were calculated using -3dB point spread function width of the final generated images. Both theoretical resolutions were calculated using (7) and (8). Applying experimental values to both equations, the theoretical azimuth resolution and range resolution results were 0.218m and 1.000m respectively. Results from the experiment indicate that the plate has better azimuth resolution than the dihedral in all channels. This is because the dihedral corner reflector has relatively strong dependency for incidence angle, and thus misalignment was frequently occurred. The results also indicate the range resolution differences according to the polarization channels. In case of larger resolution image, it is thought that mixing of desired scattering and multi-path scattering was happened. In addition, use of antennas which has narrow bandwidth is also problem. Therefore, to achieve high resolution image, precise setting of corner reflector and use of the broadband antenna is required.

TABLE III SAR SYSTEM PARAMETER VALUES USED IN THE EXPERIMENT: THE ATTENUATORS ARE INTERNAL COMPONENTS OF THE RF TRANSMITTER

Category	Value
Bandwidth	150 MHz
Pulse Duration Time	2 s
Receiving Time	3 s
Number of Pulses	51
Total Attenuation	68 dB

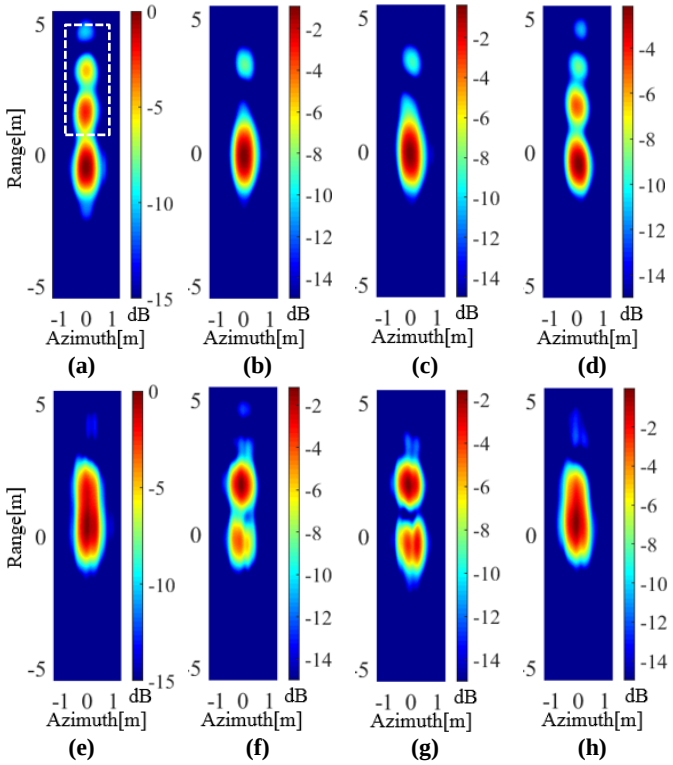

Figure 11 CP-SAR images generated from 51 azimuth interval points. (a)-(d) and (e)-(h) show plate reflector and dihedral reflector results respectively. (a) LL, (b) RR, (c) RL (e) RR (d) LL, (f) LR, (g) RL, and (h) RR configuration are shown

TABLE IV CALCULATED AZIMUTH RESOLUTIONS AND RANGE RESOLUTIONS FROM THE FINAL IMAGES

	Plate		Dihedral	
	Azimuth[m]	Range[m]	Azimuth[m]	Range[m]
LL	0.587	1.361	0.709	2.800
LR	0.583	1.656	0.628	1.189
RL	0.614	1.688	0.706	1.157
RR	0.630	1.383	0.663	2.337

IV. CONCLUSION

We developed a new L-band CP-SAR system to overcome drawbacks of conventional LP-SAR. The developed CP-SAR system is comprised of PC, FPGA, ADC/DAC converter, RF transmitter/receiver, and circularly polarized micro-strip patch array antennas. The DDS chirp signal generator was chosen since it can change the chirp signal bandwidth flexibly without large ROM size. The implemented DDS chirp signal generator was verified after measuring its performance at both output of the DAC and the RF transmitter, with 150MHz bandwidth and 10μs pulse duration time. SAR full polarimetric imaging experiment in an anechoic chamber was conducted using two types of aluminum canonical reflectors to verify the developed system performance. Developed CP-SAR system could generate SAR images of both targets in every polarization channels. The generated results indicate that the necessity of

antenna with good AR. Therefore, further improvement of micro-strip patch array antenna is anticipated. The proposed CP-SAR system is a first step towards fundamental polarimetric study of the CP-SAR and development of small satellite and UAV onboard CP-SAR system.

ACKNOWLEDGMENTS

Josaphat Microwave Remote Sensing Laboratory (JMRSL) thanks to the Japanese Ministry of Education and Technology (Monbukagakusho); Japan Science and Technology Agency (JST) for Science and Technology Research Partnership for Sustainable Development (SATREPS) Program, Chiba University–Venture Business Laboratory (VBL) etc for supporting the research.

REFERENCES

[1] A. Freeman and S. S. Saatchi, "On the detection of Faraday rotation in linearly polarized L-band SAR backscatter signatures," *IEEE Transactions on Geoscience and Remote Sensing*, vol. 42, no. 38, pp. 1607–1616, 2004. CrossRef

[2] A. Rosenqvist, M. Shimada, N. Ito, and M. Watanabe, "ALOS PALSAR: A Pathfinder Mission for Global-Scale Monitoring of the Environment," *IEEE Transactions on Geoscience and Remote Sensing*, vol. 45, no. 11, pp. 3307-3316, 2007. CrossRef

[3] Y. -L. Desnos, C. Buck, J. Guijarro, G. Levrini, J. -L. Suchail, R. Torres, J. Closa, and B. Rosich, "The ENVISAT advanced synthetic aperture radar system," *In Proc. IEEE International Symposium on Geoscience and Remote Sensing Symposium (IGARSS)*, vol. 3, pp. 1171-1173, 2000. CrossRef

[4] ITU, *Handbook on Satellite Communication*, 3th ed. New York, USA: Wiley, 2002.

[5] R. Touzi, "On the use of polarimetric SAR data for ship detection," *In Proc. IEEE International Symposium on Geoscience and Remote Sensing Symposium (IGARSS)*, pp. 812–814, 1999. CrossRef

[6] P. R. Akbar, J. T. S-Sumantyo, and H. Kuze, "A novel circularly polarized synthetic aperture radar (CP-SAR) system onboard a spaceborne platform," *International Journal of Remote Sensing*, vol. 31, no. 4 pp. 1053-1060, 2009. CrossRef

[7] J. T. Sri-Sumantyo, "Development of Circularly Polarized Synthetic Aperture Radar (CP-SAR) Onboard Small Satellite," *Progress In Electromagnetics Research Symposium (PIERS) Proceeding*, pp. 334-341, 2011.

[8] P. C. Pedersen, "Digital generation of coherent sweep signals," *IEEE Transactions on Instrumentation and Measurement*, vol. 39, no. 1, pp. 90-95, 1990. CrossRef

[9] M. Y. Chua and V. C. Koo, "FPGA-based Chirp Signal Generator for High Resolution UAV SAR," *Progress In Electromagnetics Research (PIER)*, vol. 99, pp. 71-88, 2009. CrossRef

[10] H. Yang, J. T. S. Sumantyo, J. -H. An, H. -W. Jung, and J. -H. Kim, "Phase Error Compensation Method Using Polynomial Model for A Digital Synthesizer Based Chirp signal generator," *In Proc. IEEE International Symposium on Geoscience and Remote Sensing Symposium (IGARSS)*, pp. 786–789, 2015. CrossRef

[11] A. S. Samarah, "A Digital Sweep (chirp) Generator With Extremely Small Memory Size And High Level Of The Spurious Free Dynamic Range," *International Journal of Simulation Systems, Science & Technology (IJSSST)*, vol. 11, no. 1, pp. 9-15, 2010.

[12] H. Yang, G. F. Panggabean, A. Hendra, B. Purbantoro, C. E. Santosa, K. Nakamura, Y. Izumi, J. T. S. Sumantyo, and K. –R. Kim "Conceptual Design of High-Resolution X-band Unmanned Aerial Vehicle (UAV) On-board Synthetic Aperture Radar." *Progress in Communication and Sciences*, vol. 2, no. 1, pp. 14-22, 2015.

[13] Yohandri, B. Wissan, I. Firmansyah, P. R. Akbar, and J. T. S. Sumantyo, "Development of Circularly Polarized Array Antenna for Synthetic Aperture Radar Sensor Installed on UAV," *Progress In Electromagnetics Research (PIER)* ,vol. 19, pp. 119-133, 2011. CrossRef

[14] H. Rudolf, D. Tarchi, and A. J. Siever, "Combination of Linear and Circular SAR for 3-D Features," *In Proc. IEEE International Symposium on Geoscience and Remote Sensing Symposium (IGARSS)*, vol. 4, pp. 1551-1553, 1997. CrossRef

[15] M. A. Richard, *Fundamentals of Radar Signal Processing*, 2nd Ed. New York, USA, McGraw-Hill, 2005.

[16] C. Ozdemir, *Inverse Synthetic Aperture Radar Imaging with MATLAB Algorithm*, 1st Ed. New York, USA: Wiley, 2012. CrossRef

[17] W. L. Stutzman, *Polarization in Electromagnetic Systems*, 1st Ed. Norwood, USA, Artech House, 1993.